LIGHT CURVE SIMULATION USING SPACECRAFT CAD MODELS AND EMPIRICAL MATERIAL SPECTRAL BRDFS

Alex Willison*, Donald Bédard†
Royal Military College of Canada, Kingston, Canada

Abstract

Spectrometric observations of spacecraft in Earth orbit are difficult to obtain, limiting surface composition characterization to the interpretation of photometric measurements. Accurate modelling of spacecraft spectral reflectance is therefore required to simulate quantities that can be used towards confident interpretation. This paper presents a Matlab-based system to model the spectral reflectance of spacecraft, represented as an overall spectral bidirectional reflectance distribution function (sBRDF), by applying a spacecraft's surface material reflectance characteristics to its computer-aided design (CAD) model. The broadband bidirectional reflectance distribution function (BRDF) is produced by integrating the sBRDF over the optical wavelength range, while colour-filtered BRDFs are produced by first multiplying the sBRDF by colour-filter transmittance functions and integrating the products. These quantities provide the basis of photometric light curves.

The modelling system, currently unnamed, uses triangular-faceted CAD models and colour-material definitions to represent complex spacecraft. It refers to empirical sBRDF look-up tables that have been developed from the limited measurements of homogeneous spacecraft materials using interpolation and extrapolation methods. The synthesis of overall spacecraft sBRDF is accomplished using a geometric approach, where individual facet contribution is proportional to the relative area of its orthogonal projection to the observer.

The first spacecraft to be modelled using this system was the Canadian Advanced Nanospace eXperiment 1 (CanX-1) Engineering Model (EM) nanosatellite. The synthetic sBRDF and simulated BRDF are compared with the measured reflectance spectrum and photometric light curve of the spacecraft, collected during an optical ground truth characterization experiment, in order to demonstrate the system's validity and utility towards surface composition characterization. The Matlab-based system is being extended to simulate photometric light curves of spacecraft in Earth orbit using Two-Line-Element (TLE) sets, yaw/pitch/roll angles, and observer lat/lon/alt position. Measured light curves of the Near-Earth Object Surveillance Satellite (NEOSSat) will be used to validate simulated quantities.

1 INTRODUCTION

Reflectance spectroscopy was established by the astronomical community for the surface composition characterization of asteroids[1]. Unfortunately, spectrometric observations of spacecraft in Earth orbit are much more difficult to obtain. The surfaces of artificial resident space objects are more complex and their illumination and observation geometry is constantly changing; these factors affect the spectrum of reflected light. Combined with the limited size of space surveillance-tasked telescopes, it is difficult to achieve a significant signal-to-noise ratio for spectrometric measurements [2]. As a result, current space surveillance ability limits surface composition characterization to the interpretation of photometric measurements. Accurate modelling of spacecraft spectral reflectance is therefore required to simulate quantities that can be used for confident interpretation.

The optical ground truth characterization of a spacecraft is the collection of *a priori* knowledge consisting of its physical dimensions, material composition, and the reflectance of its component materials [3]. This characterization serves as a basis against which all photometric measurements of the spacecraft in Earth orbit are compared. The method to characterize a spacecraft's optical ground truth is to completely illuminate it

*Research Assistant, Space Surveillance Research Laboratory, Department of Physics, alex.willison@rmc.ca
†Major, Space Surveillance Research Laboratory, Department of Physics, donald.bedard@rmc.ca

using a collimated light source and take measurements using a far-field camera [4]. Performed in a controlled environment, this allows for the closest recreation of the conditions under which the spacecraft will be illuminated and observed while orbiting Earth. Three difficulties present themselves when attempting to obtain an optical ground truth characterization in this manner:

1. Measurements must be made for as many different orientations as possible to reproduce the expected illumination and observation geometries in orbit.
2. Larger spacecraft are more difficult to illuminate uniformly with a collimated light source, as well as observe with a far-field detector.
3. Access to a subject prior to launch can be difficult to obtain, particularly with respect to short mission timelines.

The spectrum of a spacecraft is a combination of the individual spectra of its component materials, where contribution is proportional to relative abundance [5]. A method to synthesize the optical ground truth characterization of a spacecraft is to apply its material reflectance characteristics to its computer-aided design (CAD) model [3]. This avoids the difficulties of the laboratory characterization method as it is less arduous to determine the reflectance of material samples: obtaining, manipulating, illuminating, and observing them is more straightforward than an entire spacecraft.

The work that is presented here was conducted to develop a system to model the spectral reflectance of spacecraft, essentially simulating their optical ground truth characterization. It outlines the representation of spacecraft using triangular-faceted CAD models and the development of empirical sBRDF look-up tables from limited measurements of homogeneous materials. This type of system may be used to interpret the photometric measurements made of spacecraft in Earth orbit without requiring their complete optical ground truth characterization before launch. Such a system may also be used as a predictive tool to plan observation missions. The optical ground truth characterization of the Canadian Advanced Nanospace eXperiment 1 (CanX-1) Engineering Model (EM) nanosatellite is used to validate the spectral reflectance model, as well as demonstrate its use towards space surveillance.

2 THE SPECTRAL BRDF AND ITS DERIVATIVES

This section provides the conceptual knowledge pertaining to this research and the system to model the spectral reflectance of spacecraft. It introduces illumination and reflection geometry and defines the spectral bidirectional reflectance distribution function (sBRDF). The derivatives of the sBRDF are also outlined, including the broadband bidirectional distribution function (BRDF), colour-filtered BRDFs, and colour ratios. The measured sBRDF and subsequent BRDFs of three homogeneous spacecraft materials are presented for reference and visual interpretation of the experimental results later in this paper.

2.1 THE SPECTRAL BRDF

Illumination and reflection geometry is defined by six angles [6], shown in Fig. 1. Illumination angles are denoted by subscript i and reflection angles are denoted by subscript r. θ_i and θ_r are the polar angles measured from the surface normal vector, $\vec{N}$, to the illumination and reflection vectors, respectively. ϕ_i and ϕ_r are the azimuth angles measured from an arbitrary axis in the surface plane. Finally, ω_i and ω_r are the solid angles subtended by the illumination source and reflection beam.

The bidirectional reflectance distribution function, $f_r\left(\theta_i, \phi_i; \theta_r, \phi_r; \lambda\right)$, is defined by Nicodemus et al. [6] as "the ratio of the reflected radiance from a surface in a given direction to the incident radiance from a given direction, as a function of wavelength per unit steradian". Schaepman-Strub et al. [7] introduced the term *spectral* bidirectional reflectance distribution function (sBRDF) to highlight its dependency on wavelength, λ, emphasizing that it is a spectrometric quantity. This relationship is provided in Eq. 1 [6, 7]:

$$f_r\left(\theta_i, \phi_i; \theta_r, \phi_r; \lambda\right) = \frac{dL_r\left(E_i; \theta_i, \phi_i; \theta_r, \phi_r; \lambda\right)}{L_i\left(\theta_i, \phi_i; \lambda\right) \cdot \cos\theta_i \cdot d\omega_i} \quad \left[\mathrm{sr}^{-1}\right] \tag{1}$$

where L_i and L_r are the incident and reflected radiance, respectively. Note that the sBRDF is independent of surface area.

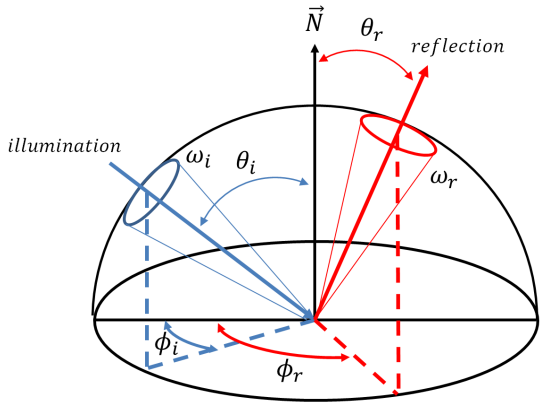

Fig. 1: The illumination and reflection geometry of an infinitesimal area, defined by its surface normal vector.

An analysis of the sBRDFs of homogeneous materials commonly found on spacecraft surfaces was performed by Bédard et al. [8] to better understand how material spectra changed as a function of illumination and observation geometry. The materials analyzed included aluminum alloy, two types of triple-junction photovoltaic (TJPV) cell, white paint, and multi-layer insulation (MLI). It was shown in [8] that material sBRDFs change with illumination and observation geometry: increasing θ_i causes an increase in sBRDF magnitude; for some materials, increasing θ_i causes spectral features to shift towards shorter wavelengths; and a single sBRDF may not be used to represent an entire material class as individual samples exhibit their own distinct sBRDF, allowing for differentiation of samples within the same material class.

The sBRDFs of Emcore TJPV cell, 6061-T6 aluminum alloy, and Lord Aeroglaze 276A reflective white low-outgassing paint are presented in Fig. 2 for a few illumination and observation geometries. Fig. 2a shows the characteristic thin-film interference features between 600 and 800 nm of Emcore TJPV cell, while Fig. 2b depicts the 800 nm absorption feature characteristic of aluminum. The spectral reflectance of Lord Aeroglaze 276A reflective white low-outgassing paint, provided in Fig. 2c, is relatively uniform across all wavelengths. Note that sBRDF of both aluminum and white paint depict the relationship between θ_i and magnitude of reflectance.

2.2 DERIVATIVES OF THE SPECTRAL BRDF

The *broadband* bidirectional reflectance distribution function (BRDF), $f_r\left(\theta_i, \phi_i; \theta_r, \phi_r\right)$, a term first used by Bédard et al. [8], is derived from the sBRDF. It is produced by integrating the sBRDF over a wavelength range, making it a photometric quantity. Eq. 2 provides the relationship between the BRDF and sBRDF [8].

$$f_r\left(\theta_i, \phi_i; \theta_r, \phi_r\right) = \sum_{\lambda_1}^{\lambda_2} f_r\left(\theta_i, \phi_i; \theta_r, \phi_r; \lambda\right) \cdot \Delta\lambda \quad \left[\mathrm{sr}^{-1}\right] \tag{2}$$

The BRDF has been used in many ways by different authors, often with confusion. The naming convention of *spectral* and *broadband* BRDF was adopted in [8] to promote their differentiation. In keeping with this convention, the spectral BRDF is denoted as sBRDF and the broadband BRDF as BRDF for the remainder of this paper.

Colour-filtered BRDFs are produced by multiplying the sBRDF by the Bessel [9] colour-filter transmittance functions and integrating the products. This mathematical relationship is shown in Eq. 3:

$$f_r\left(\theta_i, \phi_i; \theta_r, \phi_r\right)_{colour} = \sum_{\lambda_1}^{\lambda_2} T_{colour}\left(\lambda\right) \cdot f_r\left(\theta_i, \phi_i; \theta_r, \phi_r; \lambda\right) \cdot \Delta\lambda \quad \left[\mathrm{sr}^{-1}\right] \tag{3}$$

where $T_{colour}\left(\lambda\right)$ is a colour-filter transmittance function.

Colour ratios are calculated using Eq. 4, where one colour-filtered BRDF is divided by another.

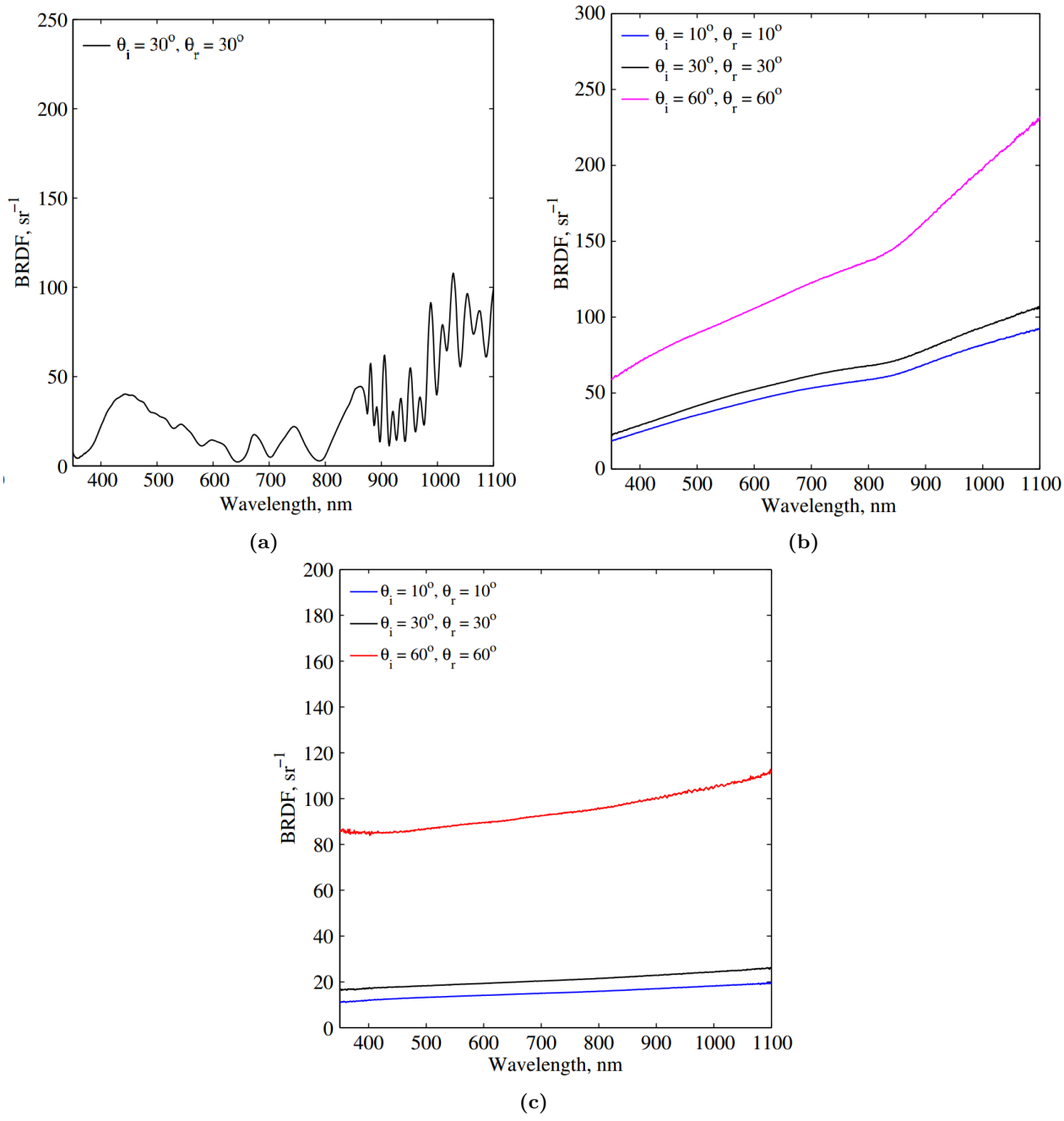

Fig. 2: The sBRDF of (a) Emcore TJPV cell, for one illumination and observation geometry, and (b) 6061-T6 aluminum alloy and (c) Lord Aeroglaze 276A reflective white low-outgassing paint, for three illumination and observation geometries.[8]

$$Ratio_{colour_1/colour_2} = \frac{f_r\left(\theta_i, \phi_i; \theta_r, \phi_r\right)_{colour_1}}{f_r\left(\theta_i, \phi_i; \theta_r, \phi_r\right)_{colour_2}} \tag{4}$$

The normalized BRDFs and colour ratios of Emcore TJPV cell, 6061-T6 aluminum alloy, and Lord Aeroglaze 276A reflective white low-outgassing paint for one θ_i value are presented in Fig. 3. Note that each point on the BRDF curve is an integrated sBRDF. The aluminum is the least specular material as the width of its BRDF is greater than 15°, while the Emcore cell is the most specular with a BRDF width of approximately 1°. The colour ratios of the aluminum and white paint were fairly uniform across the BRDF, while those of the Emcore cell were more "U"-shaped.

3 MODELLING SPACECRAFT SPECTRAL REFLECTANCE

This section describes a system to model a spacecraft's spectral reflectance as an overall sBRDF. It begins by presenting the system architecture and required inputs. The representation of spacecraft using triangular-faceted CAD models is described, including the use of colour to define component materials. Next, angles are redefined and modified as required for the empirical sBRDF look-up tables utilized by the modelling system. A description of the development of these empirical sBRDF look-up tables is provided. This section concludes by outlining the synthesis of overall spacecraft sBRDF and the subsequent production of BRDFs, colour-filtered BRDFs, and colour ratios.

3.1 SYSTEM ARCHITECTURE

The sBRDF of a spacecraft is synthesized by a Matlab-based modular system, currently unnamed. Fig. 4 provides an overview of the system architecture. Required inputs are the illumination and observation positions, a triangular-faceted CAD model of the spacecraft, colour-material definitions, and empirical sBRDF look-up tables of the spacecraft's homogeneous surface materials. The main product of this system is the overall sBRDF which is used to produce BRDFs, colour-filtered BRDFs, and colour ratios.

This system was designed for future incorporation of additional modules, thereby increasing its ability to model the spectral reflectance of spacecraft and to produce quantities useful for space surveillance. Its development in Matlab serves to ensure that it is accessible, customizable, and readily interpreted.

3.2 SPACECRAFT REPRESENTATION

Spacecraft are represented using triangular-faceted CAD models based on the STereoLithography (STL) format, where matrices define facet characteristics. Details about these matrices, along with examples, are provided in Tab. 1. The facet represented by these matrices is shown in Fig. 5. Note that the red-green-blue (RGB) data is manually added to the STL files after export from CAD software as they do not natively incorporate colour.

Tab. 1: The four matrices of a CAD model facet.

Matrix	Name	Description	Example
V	Vertices	3D Cartesian coordinates	$\begin{bmatrix} 0 & 0 & 0 \\ 0 & 0.5 & 0.5 \\ 0 & 0.5 & -0.5 \end{bmatrix}$
F	Facet	Vertex connection order	$\begin{bmatrix} 1 & 2 & 3 \end{bmatrix}$
N	Surface normal	Unit vector	$\begin{bmatrix} 1 & 0 & 0 \end{bmatrix}$
C	Colour	Facet RGB values	$\begin{bmatrix} 1 & 0 & 0 \end{bmatrix}$

The material composition of a facet is defined by its RGB values, of which there are millions of possible combinations, allowing for the incorporation of as many materials within this system. A facet's colour is used

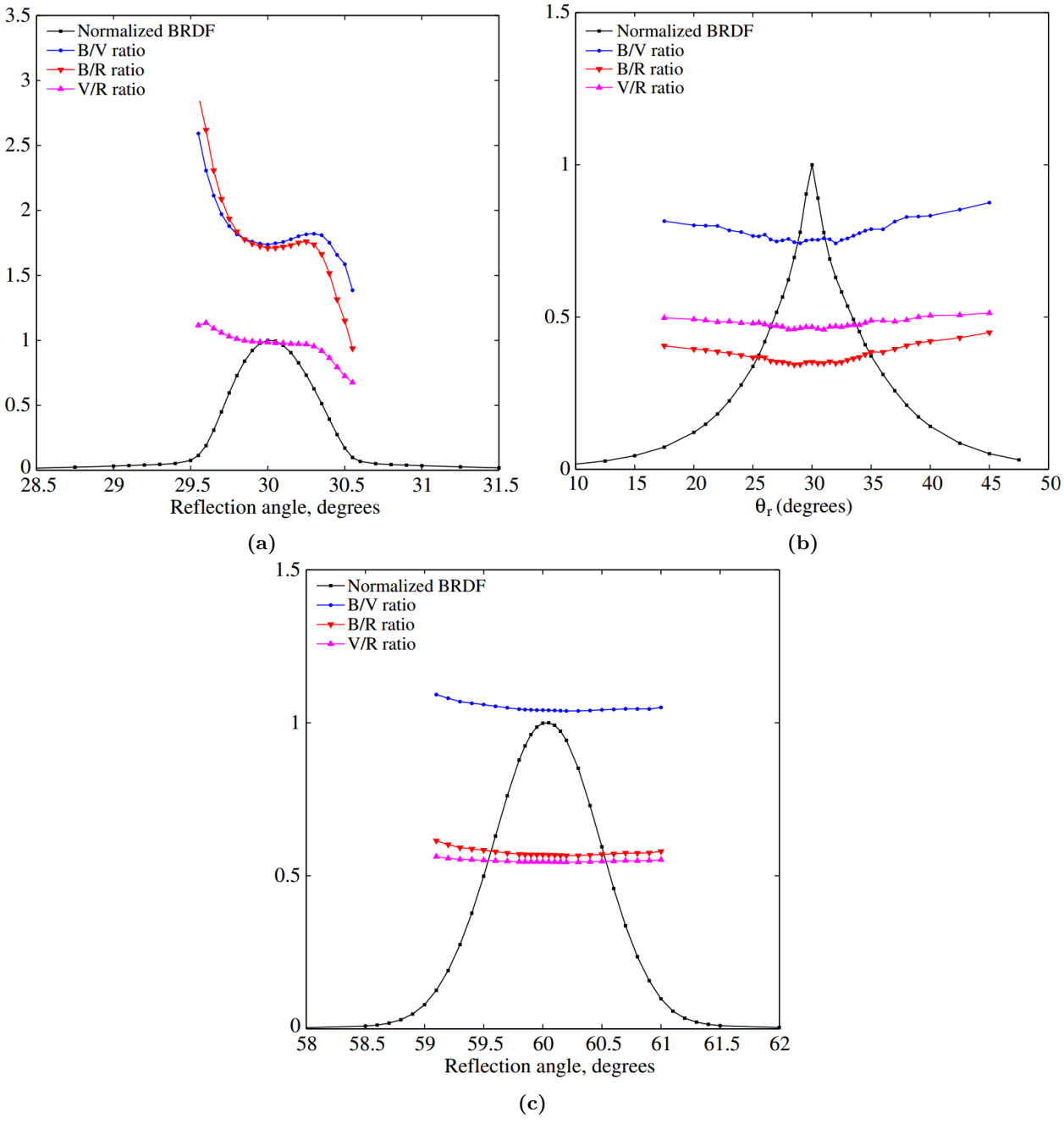

Fig. 3: The normalized BRDF and colour ratios of (a) Emcore TJPV cell and (b) 6061-T6 aluminum alloy for $\theta_i = 30°$, and (c) Lord Aeroglaze 276A reflective white low-outgassing paint for $\theta_i = 60°$.[8]

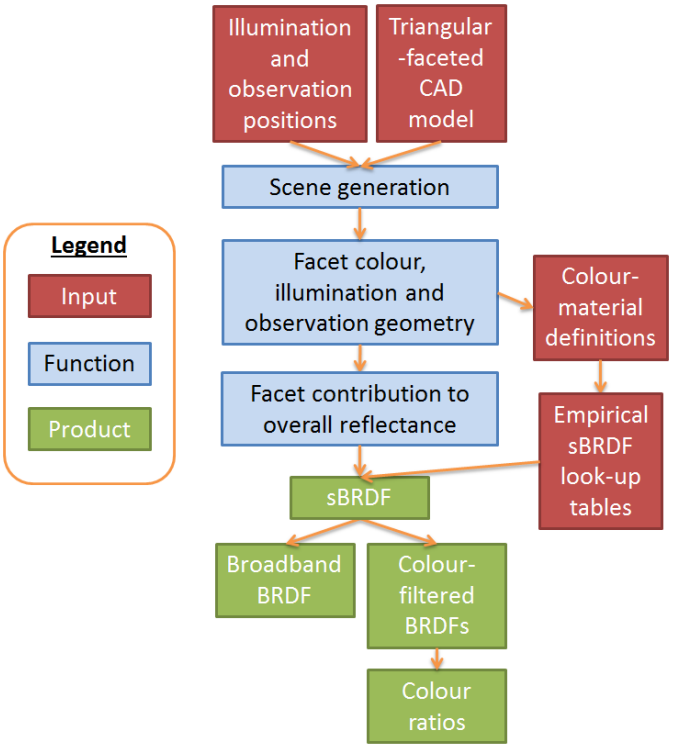

Fig. 4: The architecture of the Matlab-based modular system to synthesize the overall sBRDF of spacecraft.

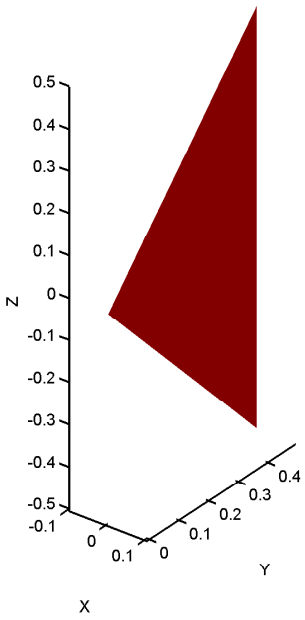

Fig. 5: The facet represented by the matrices in Tab. 1

to determine which material sBRDF look-up table to access. Tab. 2 shows the colour-material definitions used during this research.

Tab. 2: The colour-material definitions.

RGB Values	Colour	Material
$\begin{bmatrix}1 & 0 & 0\end{bmatrix}$	red	6061-T6 aluminum alloy
$\begin{bmatrix}0 & 0 & 1\end{bmatrix}$	blue	Emcore TJPV cell
$\begin{bmatrix}1 & 1 & 1\end{bmatrix}$	white	Lord Aeroglaze 276A reflective white low-outgassing paint

3.3 REDEFINITION AND MODIFICATION OF ANGLES

The angles defined in Section 2 required redefinition and modification for this system. A single illumination vector results in many reflection vectors due to the directional- and uniform-diffuse components of reflection, meaning there can be multiple reflected polar and azimuth angles, θ_r and ϕ_r, for one illumination position. Since the objective was to synthesize the overall sBRDF of a spacecraft as viewed by an observer, the removal of the reflection vectors and introduction of an observation vector was performed. This resulted in single values for θ_o and ϕ_o, the observer polar and azimuth angles, for which the overall spacecraft sBRDF would be synthesized.

The calculation of the illumination and observation azimuth angles, ϕ_i and ϕ_o, requires the definition of an axis in the surface plane from which both are measured. This axis may be arbitrarily defined, making the azimuth angles relative. The difference between them, $\Delta\phi$, is therefore a more useful quantity. This *difference-in-azimuth* angle is indicative of whether θ_o is in the plane defined by θ_i. A $\Delta\phi$ value of 0° or 180° means θ_o is in-plane, while all other values indicates that it is off-plane. It is important to note that all the material sBRDF measurements presented in [8] were obtained for a $\Delta\phi$ value of 180° as θ_o was in-plane and on the opposite side of $\vec{N}$ from θ_i.

The illumination and observation angles used by this system, including the difference-in-azimuth angle, are shown in Fig. 6a. Note that the solid angles, ω_i and ω_o, were removed as the illumination source and observer are defined as points.

An angular conversion required to develop empirical sBRDF look-up tables from the limited laboratory measurements presented in [8] was to convert θ_o to the equivalent *angle-off-specular*, θ_{os}, shown in Fig. 6b. A negative value of θ_{os} indicates that the phase angle, β, is less than $2\theta_i$ and a positive value indicates that β is greater than this value, assuming that θ_o is in-plane. After making the redefinition and modification of angles the sBRDF is now a function of these angles, $f_r\left(\theta_i; \theta_{os}; \Delta\phi; \lambda\right)$.

3.4 DEVELOPMENT OF EMPIRICAL SBRDF LOOK-UP TABLES

The material sBRDFs in [8] were developed into empirical sBRDF look-up tables for this system. This was done to avoid the use of theoretical BRDF models while ensuring that observed material spectral reflectance characteristics were maintained.

Three homogeneous material sBRDFs, each obtained for three θ_i values, were initially selected for this system. The sBRDFs were originally measured across the entire reflected beam with zero reflectance observed beyond this range. The increment in observation angle was adjusted to obtain more detail near specular. The highest observation angle resolution was achieved for the Emcore TJPV cell as it was a highly specular reflector while the lowest observation angle increment was achieved for the 6061-T6 aluminum alloy which was the least specular.

The development of empirical sBRDF look-up tables from these limited laboratory measurements required two steps. First, the material sBRDFs needed to be established for all θ_o. As the smallest observation angle increment was $\Delta\theta_o = 0.05°$ for the Emcore TJPV cell, a linear interpolation of all measured sBRDFs was performed with the same increment to maintain this fidelity. This interpolation was conducted for all wavelengths, for each of the θ_i values of the measured homogeneous material sBRDFs. At this point the

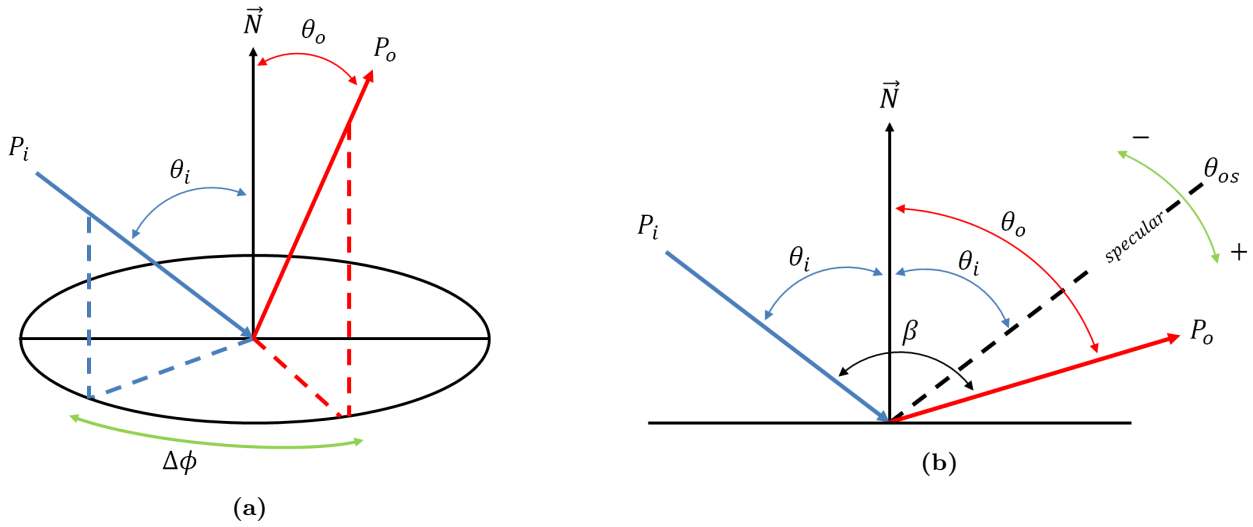

Fig. 6: (a) The illumination and observation angles used by this system, and (b) the relationship between θ_i, θ_o, and θ_{os}, where all angles are in the same plane. β is included for interpretation.

sBRDFs were converted from functions of θ_o to θ_{os}, where $\Delta\phi = 180°$. Fig. 7a shows the measured sBRDF of 6061-T6 aluminum alloy for one θ_i and wavelength, along with the empirical sBRDF produced by linear interpolation, both as functions of θ_{os}. The second step to develop the empirical sBRDF look-up tables was to interpolate and extrapolate the sBRDFs for all θ_i using a cubic spline curve fit with a 1° interval. This interpolation and extrapolation was conducted for all wavelengths, for each of the θ_{os} values of the measured/linearly-interpolated sBRDFs. Fig. 7b shows the measured/linearly-interpolated sBRDF of 6061-T6 aluminum alloy for one θ_{os} and wavelength, along with the empirical sBRDF produced by cubic spline curve fit, both as functions of θ_i.

A consequence of the extrapolation through cubic spline curve fit was a sBRDF increase below 10° and above 60°. It was shown in [8] that sBRDF magnitude increases with an increase in θ_i leaving the decrease from 0° to 10° in question. Conversely, while an increase is expected above 60°, the rate at which it does so is uncertain. A better cubic spline curve fit to more accurately model spectral reflectance could be achieved if sBRDFs were measured for more θ_i values. It was determined that the sBRDF look-up tables resulting from the three θ_i values would produce sufficiently accurate results for the purposes of this research, though measurements for more θ_i values will be obtained in the development of empirical sBRDF look-up tables in the future. The linear interpolation, angle conversion, and cubic spline curve fit resulted in three empirical sBRDF look-up tables, one for each homogenous material.

3.5 OVERALL SPACECRAFT SBRDF

The synthesis of overall spacecraft sBRDF is accomplished using a geometric approach. First, the illumination and observation geometry of each of the CAD model's triangular facets is determined. Illumination and observation polar angles, θ_i and θ_o, are located between a facet's surface normal vector, $\vec{N}$, and the illumination and observation vectors, $\vec{v_i}$ and $\vec{v_o}$, respectively. The difference-in-azimuth angle, $\Delta\phi$, is located between the orthogonal projections of $\vec{v_i}$ and $\vec{v_o}$ on the facet's surface, as viewed from the direction of $\vec{N}$. A conversion of facet θ_o to θ_{os} is also performed. The sBRDF of each facet's material, $f_r\left(\theta_i;\theta_{os};\Delta\phi;\lambda\right)_{material}$, is then obtained from the homogeneous material sBRDF look-up tables using its respective θ_i, θ_{os}, $\Delta\phi$, and colour values following the algorithm in Eq. 5.

$$\text{colour} \rightarrow \text{material} \rightarrow \Delta\phi \rightarrow \theta_{os} \rightarrow \theta_i \rightarrow f_r\left(\theta_i;\theta_{os};\Delta\phi;\lambda\right)_{material} \tag{5}$$

Next, individual facet contribution to the overall sBRDF is calculated using the area of its orthogonal projection to the observation position, a_{2D} using Eq. 6.

$$f_r\left(\lambda\right)_{facet} = a_{2D} \cdot f_r\left(\theta_i;\theta_{os};\Delta\phi;\lambda\right)_{material} \quad \left[\text{sr}^{-1}\right] \tag{6}$$

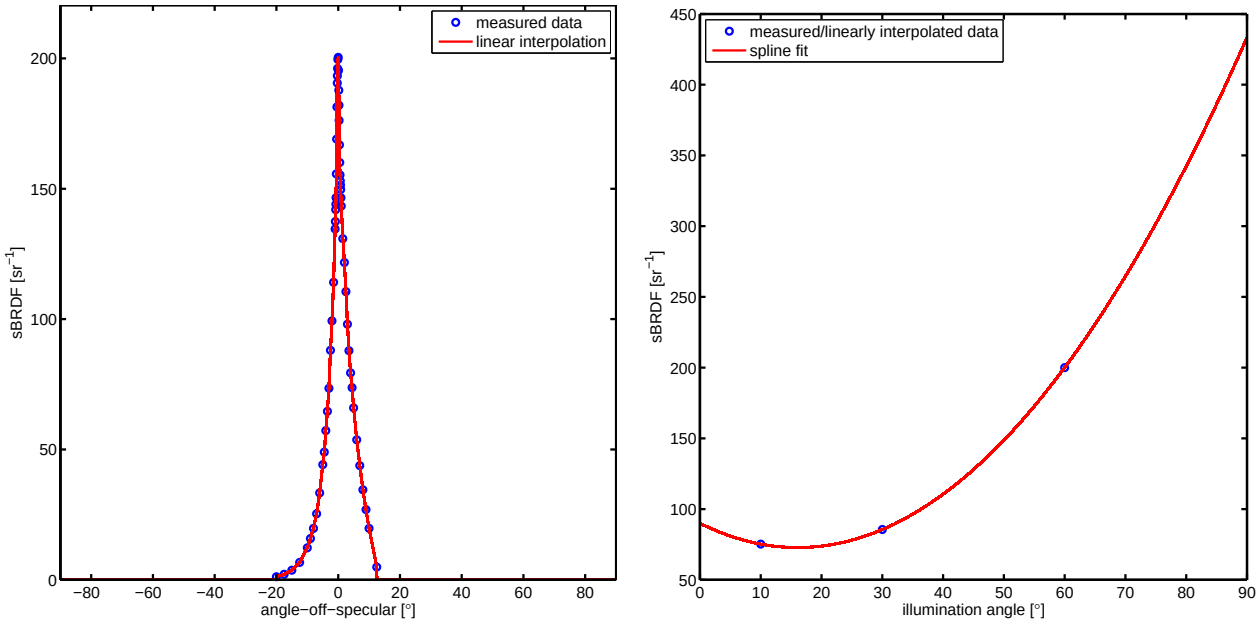

(a) **(b)**

Fig. 7: (a) The measured and linearly interpolated sBRDF of 6061-T6 aluminum alloy as a function of θ_{os} for $\theta_i = 60°$ and $\lambda = 950$ nm, and (b) the measured/linearly-interpolated and interpolated/extrapolated sBRDF of 6061-T6 aluminum alloy as a function of θ_i for $\theta_{os} = 0°$ and $\lambda = 950$ nm.

Finally, Eq. 7 describes how all facet sBRDFs are integrated and divided by the total orthographic area of the spacecraft:

$$f_r(\lambda)_{spacecraft} = \frac{\sum_{j=1}^{n} f_r(\lambda)_{facet,j}}{\sum_{j=1}^{n} a_{2D,facet,j}} \quad \left[\mathrm{sr}^{-1}\right] \tag{7}$$

where n is the total number of triangular facets contributing to the spacecraft reflectance. The sBRDF is divided by the total orthographic area to normalize the result, ensuring that its magnitude is independent of spacecraft size. The final product is the overall spacecraft sBRDF for one illumination and observation geometry.

3.6 PRODUCING DERIVATIVES OF THE OVERALL SPACECRAFT SBRDF

BRDF points are produced by integrating the overall spacecraft sBRDF over all wavelengths, for one illumination and observation geometry. BRDF curves result from performing this over the range of illumination and observation geometries contained in a simulation scenario, presented in Eq. 8:

$$f_{r\,spacecraft} = \sum_{P_i,P_o,1}^{P_i,P_o,2} \sum_{\lambda=350nm}^{1100nm} f_r(\lambda)_{spacecraft} \cdot \Delta\lambda \cdot \Delta P_i \cdot \Delta P_o \quad \left[\mathrm{sr}^{-1}\right] \tag{8}$$

where P_i and P_o are the illumination and observation positions, and subscripts 1 and 2 denote their initial and final states, respectively.

Colour-filtered BRDFs are produced by first multiplying the overall spacecraft sBRDF by the Bessel [9] colour-filter transmittance functions, resulting in filtered sBRDFs. The products are then integrated over all wavelengths, similar to the BRDF. Eq. 9 depicts the colour-filtered BRDF:

$$f_{r\,spacecraft,colour} = \sum_{P_i,P_o,1}^{P_i,P_o,2} \sum_{\lambda=350nm}^{1100nm} T_{colour}(\lambda) \cdot f_r(\lambda)_{spacecraft} \cdot \Delta\lambda \cdot \Delta P_i \cdot \Delta P_o \quad \left[\mathrm{sr}^{-1}\right] \tag{9}$$

where $T_{colour}(\lambda)$ is a Bessel [9] colour-filter transmittance function. The colour-filter transmittance functions referenced in this paper are blue (B), red (R), and infrared (I). Colour ratios are produced by dividing one colour-filtered BRDF by the other as previously shown in Eq. 4.

4 VALIDATION AND DEMONSTRATION OF THE SPACECRAFT SPECTRAL REFLECTANCE MODELLING SYSTEM

The first spacecraft to be modelled using this system was the CanX-1 EM. Simulation scenarios were designed to reproduce the experimental setup of the spacecraft ground truth characterization experiment by Bédard and Lévesque [4]. This section presents an interpretation of the synthetic overall spacecraft sBRDF and comparison with the measured reflectance factor in [4]. The interpretation of the simulated BRDF and comparison with a measured photometric light curve in [4] follows. The section concludes by interpreting the normalized simulated BRDF and associated colour ratios. This series of interpretations and comparisons is presented to demonstrate the validity of this spacecraft spectral reflectance modelling system and its potential for space surveillance characterization applications.

4.1 EXPERIMENT AIM AND OBJECTIVES

The aim of the experiment was to simulate quantities equivalent to those measured in [4] during the CanX-1 EM ground truth characterization experiment. The five main objectives of the experiment were to:

1. Interpret the synthetic sBRDF of the +X side of the spacecraft for surface composition characterization.
2. Compare the synthetic sBRDF of the +X side of the spacecraft with the measured reflectance factor.
3. Interpret the simulated BRDF of the spacecraft for surface composition characterization.
4. Compare the simulated BRDF of the spacecraft with the measured photometric light curve.
5. Interpret the colour ratios of the spacecraft for surface composition characterization.

4.2 EXPERIMENT SETUP

The experiment setup and procedure was developed to reproduce that used in [4] for the ground truth characterization of the spacecraft in a controlled environment. Access to the original CAD model could not be obtained, requiring one to be constructed. Scaled photographs, one of which is provided in Fig. 8, were used to determine the exact dimensions of the CanX-1 EM's features. This approach was chosen as it only required physical access to the spacecraft for a short period of time, a constraint of most ground truth characterization experiments.

The CAD model was constructed with measurement specifications to the tenth of a millimetre, where 1 CAD unit was equal to 1 centimetre. The model, depicted in Fig. 9, is comprised of 698 triangular facets representing one of three materials. 6061-T6 aluminum alloy and Emcore TJPV cell, respectively in red and blue, were applied to the model as these were the actual component materials of the spacecraft. Lord Aeroglaze 276A reflective white low-outgassing paint was applied to surfaces that were not aluminum or Emcore cell, as its reflectance was spectrally uniform and its inclusion within the overall spacecraft sBRDF would not affect the spectral characteristics of the other two materials.

During this experiment both illumination and observation positions were placed in the xy-plane and radially located 1000 units from the centroid of the subject. Changes in illumination and observation geometry were accomplished by rotating P_i and P_o about the spacecraft centroid in discrete angular steps, $\Delta\theta$.

Two simulations were performed for this experiment. In the first, the CAD model's orientation was fixed with its sides facing in the direction indicated by their labels. For example, the surface normal vectors of the +X side were parallel to the $+x$-axis. The +X side of the CanX-1 EM was observed for four phase angle geometries, shown in Fig. 10a, where $\beta = 2 \cdot \theta_i = 2 \cdot \theta_o = 5°$, 30°, 60° and 90°. In the second simulation, the CAD model was rotated 25° about the z-axis. The illumination and observation positions were maintained with a fixed phase angle separation of $\beta = 10°$, and were rotated 360° about the z-axis in increments of 0.1°. This simulation scenario is presented in Fig. 10b.

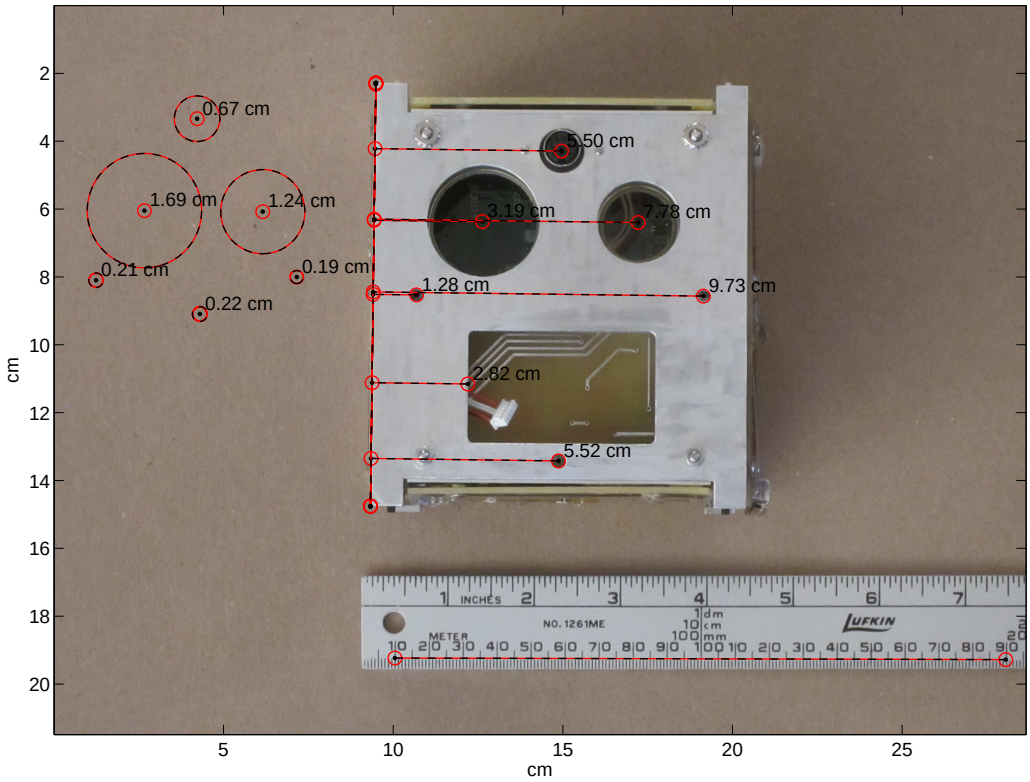

Fig. 8: A scaled photograph of the +Z side of the CanX-1 EM, with measurements.

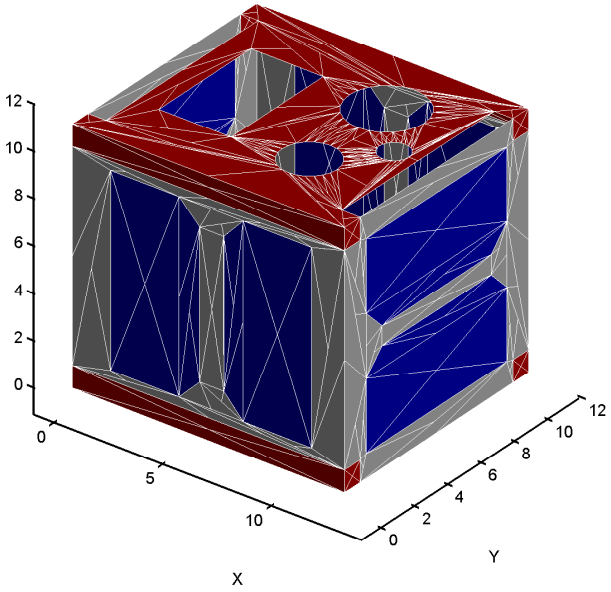

Fig. 9: The CanX-1 EM CAD model.

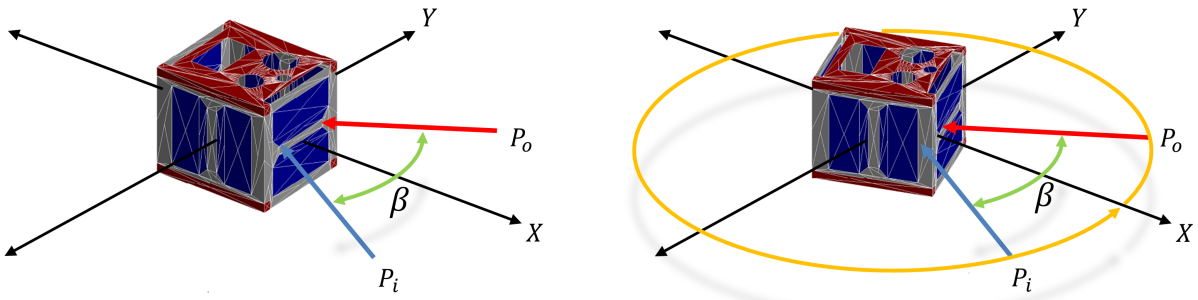

(a) (b)

Fig. 10: The (a) phase angle, and (b) fixed-phase simulation scenarios.

4.3 RESULTS

4.3.1 INTERPRETING THE SYNTHETIC SBRDF

The synthetic sBRDF of the +X side of the CanX-1 EM for four phase angles is shown in Fig. 11a. Prominent spectral features are present in the 600 to 800 nm range and shift towards shorter wavelengths with an increase in β, equating to an increase in θ_i. These features coincide with those of Emcore TJPV cell, which were shown in [8] to shift to shorter wavelengths with an increase in θ_i. The presence of Emcore TJPV cell in the synthetic spectra was expected as the +X side of the CanX-1 EM is dominated by this material. While 6061-T6 aluminum alloy is also present on this side of the model its characteristic 800 nm absorption feature is undetectable.

The magnitude of the sBRDF decreases from $\beta = 5°$ to 30° and increases thereafter. While the decrease was not an expected phenomenon based on the conclusions reached in [8], it can be explained: this is a result of the cubic spline curve fit used to develop the material sBRDF look-up tables from limited measured sBRDFs. This effect can be reduced by incorporating more measured sBRDFs in future development of look-up tables.

4.3.2 COMPARING THE SYNTHETIC SBRDF WITH THE MEASURED REFLECTANCE FACTOR

The reflectance factor is not an equivalent quantity to the sBRDF and may not be quantitatively compared. Also, the reflectance factor does not represent the relationship between reflectance magnitude and illumination angle as the sBRDF does. That being said, they can be qualitatively compared as they are both spectrometric quantities. The synthetic sBRDF in Fig. 11a and measured reflectance factor in Fig. 11b possess similar spectral characteristics. They both contain features in the 600 nm to 800 nm range which shift to shorter wavelength with increasing θ_i, though the wavelength of these features is not the same. This is because the Emcore TJPV cells are not perfectly flat, nor are they flush to the surface of the spacecraft, as shown in Fig. 12. These characteristics were not represented by the CAD model.

The variation in sBRDF magnitude, particularly exhibited in the features located above 900 nm, is not observed in the reflectance factor. This is a result of the cubic spline curve fit used to develop the sBRDF look-up tables and can be eliminated by incorporating more measured sBRDFs in the future development of look-up tables.

4.3.3 INTERPRETING THE SIMULATED BRDF

The simulated BRDF for the fixed-phase angle simulation is shown in Fig. 13a. The peaks alternate in magnitude and are separated by 90°, due to the cubic nature of the CanX-1 EM. Each peak presents a less-specular base approximately 10° wide upon which a 1°-wide specular feature sits. This indicates that the spacecraft is composed of at least two materials, one of which is more specular than the other. The CanX-1 EM is known to possess Emcore TJPV cell and 6061-T6 aluminum alloy, materials with these reflectance characteristics.

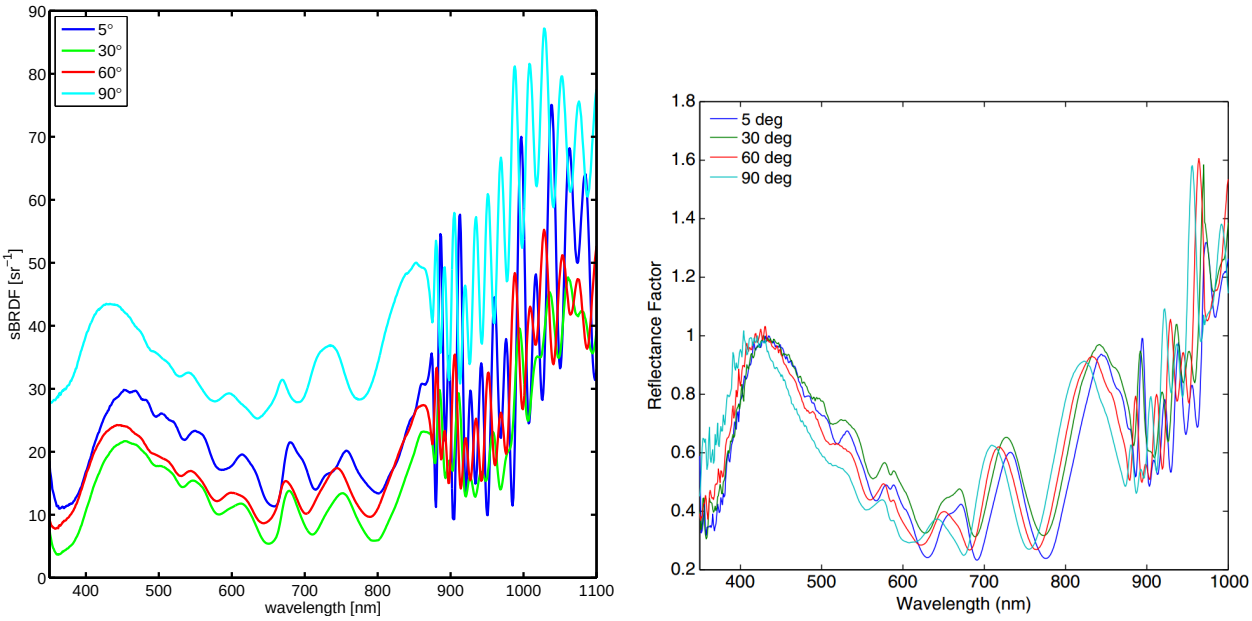

(a) (b)

Fig. 11: The (a) synthetic sBRDF, and (b) measured reflectance factor, of the +X side of the CanX-1 EM for four phase angles[4].

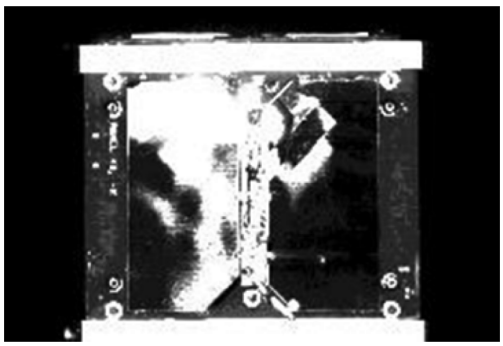

Fig. 12: An image of the CanX-1 EM, where the Emcore TJPV cells are not perfectly flat, nor are they flush to the spacecraft surface.[4]

The ordering of sides observed during the simulation was $+X \rightarrow +Y \rightarrow -X \rightarrow -Y$. The X sides exhibited less overall reflectance and shorter less-specular base features when compared to the Y sides. All four sides are known to possess the same coverage of Emcore TJPV cell; however, the X sides have noticably less 6061-T6 aluminum alloy than the Y sides. The variation in peak BRDF magnitude is therefore attributed to this difference in aluminum coverage.

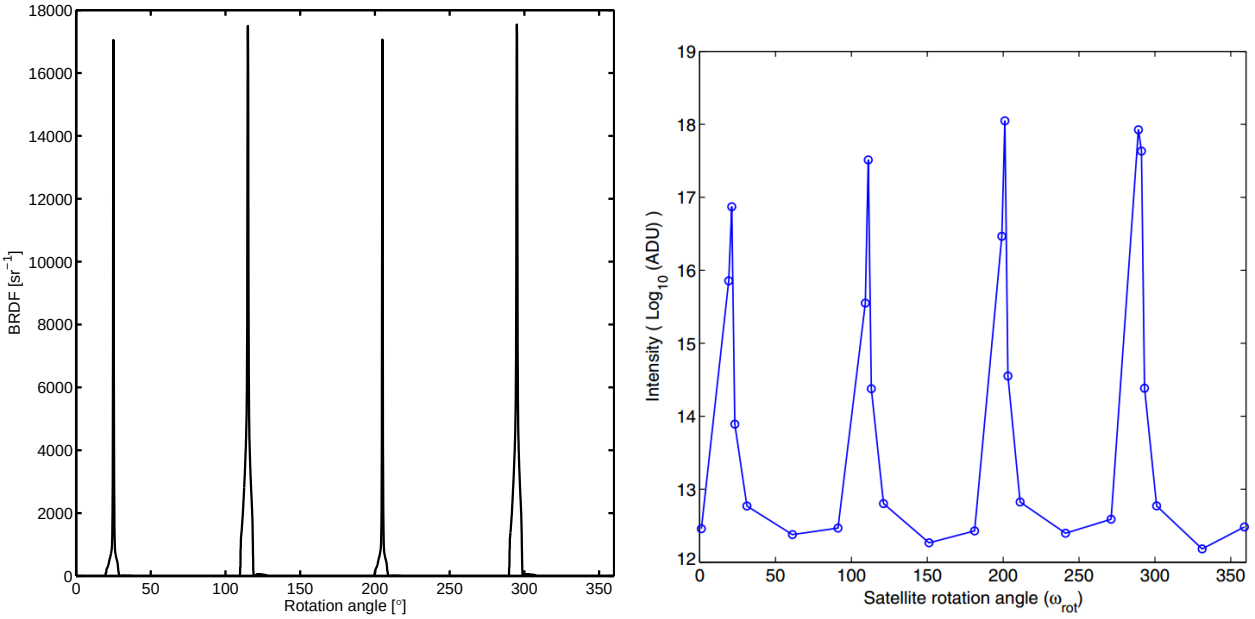

(a) **(b)**

Fig. 13: (a) The simulated BRDF, and (b) measured broadband photometric light curve [4] of the CanX-1 EM, initially rotated 25° about the z-axis, for a fixed-phase simulation where $\beta = 10°$.

4.3.4 COMPARING THE SIMULATED BRDF WITH THE MEASURED PHOTOMETRIC LIGHT CURVE

Photometric light curves and BRDFs are not equivalent quantities and may not be quantitatively compared. They can be qualitatively compared as photometric light curves are derivatives of BRDFs. The simulated BRDF and the measured photometric light curve in Fig. 13b contain similar characteristics. The specular peaks have the same angular separation of 90° and sit atop wider, less-specular base features. Conversely, the light curve does not depict the same specularity as the BRDF. This may be because measurements were made with a rotation angle increment greater than the 0.1° of the simulation, leaving uncertainty in the shape of the light curve. Additionally, the surfaces of the actual spacecraft are not perfectly flat, causing a wider rotation angle range of specular reflection. Finally, the alternating peak magnitudes and zero reflectance between the peaks of the BRDF are not observed in the light curve. This is attributed to the non-flush Emcore TJPV cells and the presence of features and diffuse materials on the surface of the spacecraft that were not represented on the CAD model.

4.3.5 INTERPRETING THE COLOUR RATIOS

Fig. 14a presents the normalized BRDF and colour ratios for the first BRDF peak, coinciding with a 25° rotation of P_i and P_o about the z-axis. The colour ratios are relatively uniform across the wider less-specular base of the BRDF. All except R/I exhibit a sharp increase near specular, where the B-band shows the greatest increase in magnitude. A discontinuity in the BRDF is located at a rotation angle of approximately 5° greater than specular. Fig. 14c presents the normalized BRDF and colour ratios for the second BRDF

peak, coinciding with a 115° rotation of P_i and P_o about the z-axis. The colour ratios behave exactly as they did for the first peak. The R/I is uniform while the greatest increase is in the B-band near specular; however, this increase is smaller in magnitude than it was for the 25° rotation angle. The discontinuity for a rotation angle of 5° greater than specular is present.

The sBRDF for five rotation angles that frame the first specular BRDF peak is presented in Fig. 14b. The sBRDF at specular, for a rotation angle of 25°, exhibits a significant number of spectral features. These diminish as the rotation angle moves away from specular until only one feature at 800 nm is present, though it is difficult to see due to scale. The sBRDF for five rotation angles that frame the second specular BRDF peak are provided in Fig. 14d. The sBRDF at specular, for a rotation angle of 115°, exhibits the same spectral features as that of 25°. These also diminish as the rotation angle moves away from specular until only the 800 nm feature is present.

The uniform colour ratios across the wider less-specular base of the normalized BRDFs in Fig. 14 are indicative of 6061-T6 aluminum alloy. The sBRDF coinciding with the rotation angles presenting these uniform colour ratios confirms the presence of 6061-T6 aluminum alloy as they depict its absorption feature. The presence of Emcore TJPV cell is responsible for the sharp increase of all colour ratios near specular excluding R/I, particularly those including the B-band. Confirmation is provided by the sBRDF located at specular which is indicative of Emcore TJPV cell, whose thin-film interference features are present. The discontinuity is caused by inaccurate data in one of the measured sBRDFs of aluminum, which will be eliminated with a reacquisition of new measurements.

A comparison of the colour ratios near specular shows a greater change in the B-band for the +X side of the spacecraft than for the +Y side. This suggests that the Emcore-cell-to-aluminum ratio is higher on the +X side of the spacecraft than on the +Y; however, the associated sBRDFs at specular say otherwise. The magnitude of Emcore TJPV cell reflectance is lesser in Fig. 14d than in Fig. 14b. Since each side is known to have the same Emcore TJPV cell coverage the only explanation for this difference is the orientation of these features: they are horizontal on the X sides and vertical on the Y. This difference is a result of using look-up tables developed from material sBRDF measurements made in-plane, where θ_o is in the plane defined by θ_i, and applying them in off-plane observation scenarios. An extension of the sBRDF look-up tables to include off-plane sBRDF data will remedy this phenomenon.

5 CONCLUSION

The system to model a spacecraft's spectral reflectance as an overall sBRDF demonstrated its ability to produce quantities that can be used to characterize spacecraft for space surveillance. The simulated quantities of the CanX-1 EM possessed qualitatively similar characteristics to those measured during the ground truth characterization of the spacecraft. These quantities were interpreted to characterize the spacecraft's surface composition.

The discrepancies between the simulated and measured quantities were sourced to two root causes. The first cause was that the CAD model did not accurately represent the spacecraft as some physical features, particularly imperfections, were excluded. This is a common limitation of CAD models. Second, the sBRDF look-up tables were derived using data from a limited number of illumination and observation geometries, which also contained errors.

While the work that was presented here was a system to model the spectral reflectance of spacecraft, photometric light curves may be calculated using the simulated broadband and colour-filtered BRDFs that it produces. With this ability, this system may be used for the interpretation of photometric measurements for surface composition characterization or as a predictive tool when planning observation missions, without requiring the complete optical ground truth characterization of a spacecraft before launch. Further development of this modelling system is being pursued to achieve such capabilities as they are becoming more crucial and define a significant step forward in the science of space surveillance.

6 FUTURE WORK

The development of look-up tables that accurately represent the spectral reflectance of materials for all illumination and observation geometries is being pursued. The focus is the determination of the required number of illumination angles and off-plane observation angles to accomplish this goal.

The system is being extended to simulate photometric light curves of spacecraft in Earth orbit using spacecraft Two-Line-Element (TLE) sets, yaw/pitch/roll angles, and observer lat/lon/alt position. Measured

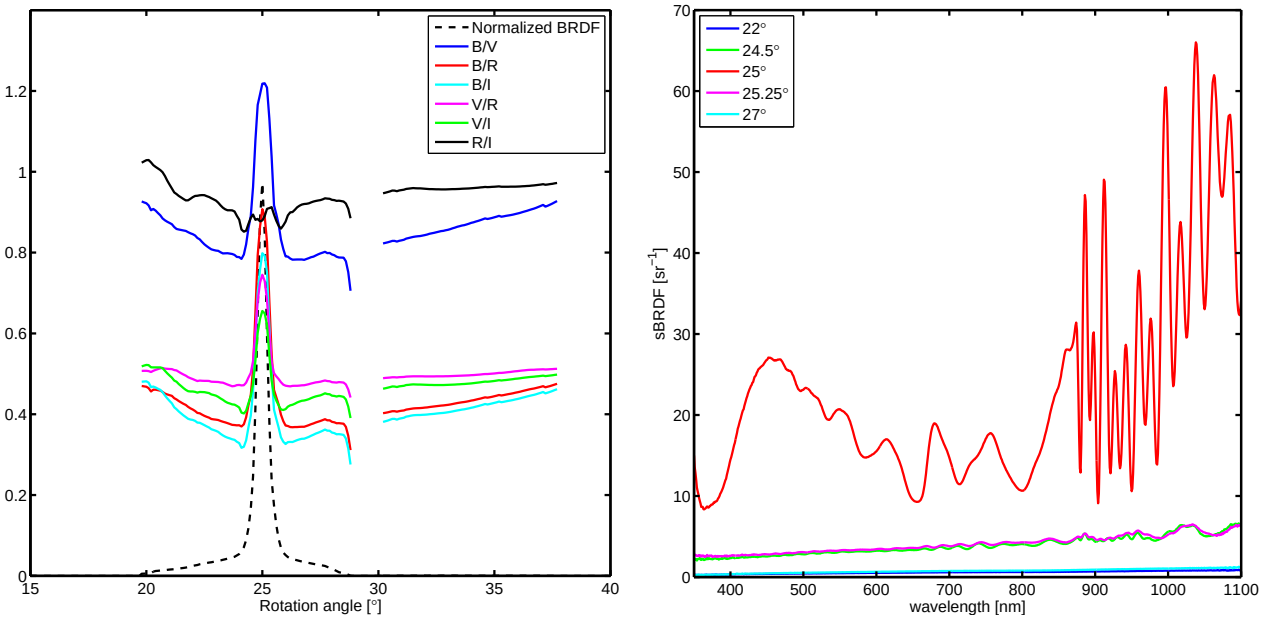

(a) (b)

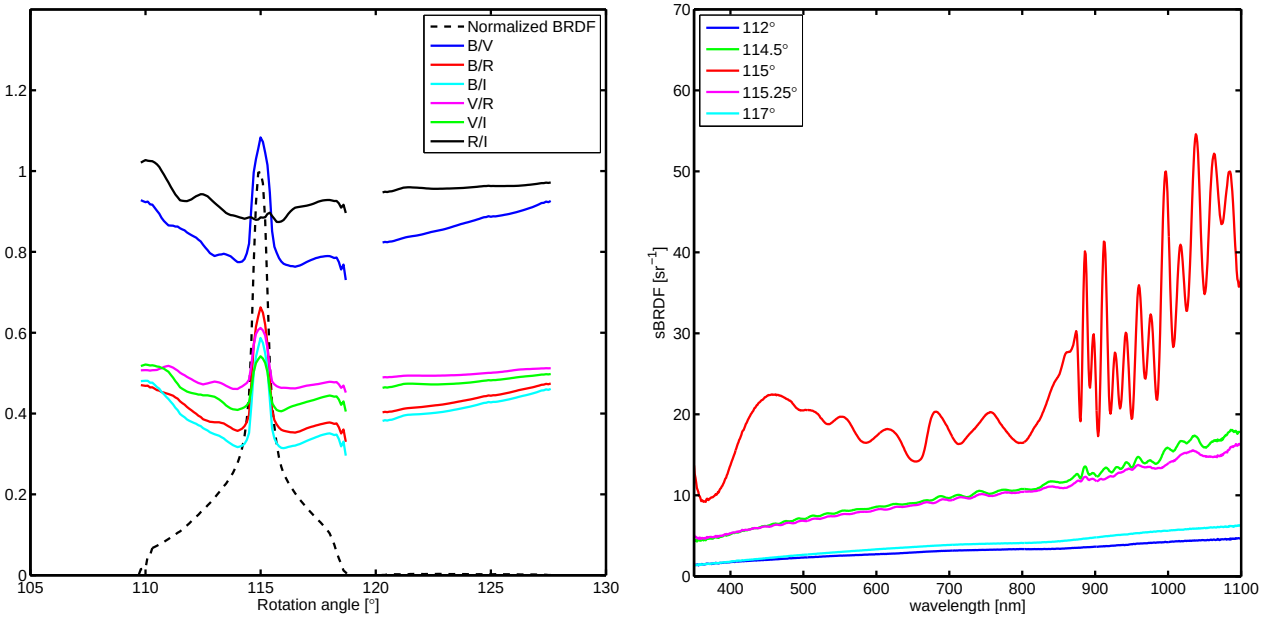

(c) (d)

Fig. 14: (a) The first peak of the normalized simulated BRDF and associated colour ratios, where specular reflectance occurs at a rotation angle of 25°, and (b) the synthetic sBRDF for five rotation angles framing the specular region. (c) The second peak of the normalized simulated BRDF and associated colour ratios, where specular reflectance occurs at a rotation angle of 115°, and (d) the synthetic sBRDF for five rotation angles framing the specular region.

light curves of the Near-Earth Object Surveillance Satellite (NEOSSat) will be used to validate simulated quantities.

Finally, the use of 3D scanning technology to measure the physical imperfections of spacecraft is being investigated. The 3D meshes that result from this method can be exported in STL format, which is used by this system.

7 References

[1] T. B. McCord, J. B. Adams, and T. V. Johnson. Asteroid Vesta: Spectral Reflectivity and Compositional Implications. *Science*, 168:1445–7, June 1970. doi: 10.1126/science.168.3938.1445.

[2] D. Bédard, G. A. Wade, and A. Jolley. Interpretation of Spectrometric Measurements of Active Geostationary Satellites. In *Proceedings of the 2014 AMOS Technical Conference*, Kihei, Maui, HI, September 2014. Maui Economic Development Board, Inc.

[3] K. Abercromby, J. Okada, M. Guyote, K. Hamada, and E. Barker. Comparisons of Ground Truth and Remote Spectral Measurement of the FORMOSAT and ANDE Spacecraft. In *Proceedings of the 2006 AMOS Technical Conference*, Kihei, Maui, HI, September 2006. Maui Economic Development Board, Inc.

[4] D. Bédard and M. Lévesque. Analysis of the CanX-1 Engineering Model Spectral Reflectance Measurements. *Journal of Spacecraft and Rockets*, 51(5):1492–1504, 2014. doi: 10.2514/1.A32643.

[5] K. K. Luu, C. L. Matson, J. Snodgrass, S. M. Giffin, K. Hamada, and J. V. Lambert. Object characterization from spectral data. In *Proceedings of the 2003 AMOS Technical Conference*, Kihei, Maui, HI, September 2003. Maui Economic Development Board, Inc.

[6] F. E. Nicodemus, J. C. Richmond, and J. J. Hsia. *Geometrical Considerations and Nomenclature for Reflectance*. U.S. Department of Commerce, Washington, D.C., October 1977.

[7] G. Schaepman-Strub, M. E. Schaepman, T. H. Painter, S. Dangel, and J. V. Martonchik. Reflectance Quantities in Optical Remote Sensing - Definitions and Case Studies. *Remote Sensing of Environment*, 103:27–42, March 2006.

[8] D. Bédard, G. A. Wade, and K. Abercromby. Laboratory Characterization of Homogeneous Spacecraft Materials. *Journal of Spacecraft and Rockets*, 52(4):1038–1056, 2015. doi: 10.2514/1.A33079.

[9] M. Bessel. UBVRI Passbands. *Astronomical Society of the Pacific*, 102:1181–1199, 1990.